LAWRENCE
LIVERMORE
NATIONAL
LABORATORY

UCRL-JRNL-214703

Improved Operation of the SSPX Spheromak

R. D. Wood, D. N. Hill, E. B. Hooper, S. Woodruff,
H. S. McLean, B. W. Stallard

August 19, 2005

Nuclear Fusion

IMPROVED OPERATION OF THE SSPX SPHEROMAK

R.D. Wood, D.N. Hill, E.B. Hooper, S. Woodruff[1], H.S. McLean, and B.W. Stallard,
Lawrence Livermore National Laboratory, Livermore

[1]Presently at the Department of Aeronautics and Astronautics, University of Washington, Seattle, WA 98195

E-mail: wood11@llnl.gov

Abstract

We present significant advances in the performance and understanding of the Sustained Spheromak Physics Experiment (SSPX). High performance discharges are obtained by adjusting the injected current and bias magnetic flux to produce a flat to slightly peaked radial current profile, consistent with reducing the drive for tearing and other MHD modes. Wall conditioning and density control also are essential to obtaining high performance discharges. With these optimizations, plasmas with peak electron temperatures of ~350 eV, edge magnetic fluctuation levels less than 1%, and core thermal diffusivities (χ_e) <10 m^2/s are produced. Most SSPX temperature data are bounded by a β_e~5% but differentiating between a stability limit and simple energy transport, until now, has not been possible. Achieving these high performance discharges enables us to consider the possibly of auxiliary heating of a spheromak for the first time.

PACS numbers: 52.55.Ip, 52.35.Vd, 52.35.Py, 52.65.Kj

1. Introduction

The spheromak is a compact self-organized toroidal plasma configuration in which confining magnetic fields are produced by poloidal and toroidal currents flowing in the plasma [1]; there are no toroidal magnetic field coils linking the plasma. A spheromak can be formed and sustained by injecting magnetic helicity ($K=\int_V \mathbf{A}\cdot\mathbf{B}dV$) from a magnetized coaxial plasma gun into a conducting confinement region (flux conserver). Through magnetic fluctuations and associated reconnection the injected plasma then relaxes into an axisymmetric toroidal geometry. The equilibrium profiles in the spheromak are nearly force free, a so-called *Taylor Relaxed State* [2]. Taylor relaxation is a dissipative process by which the plasma naturally reaches a configuration with minimum magnetic energy under the constraint that the total magnetic helicity remains constant. This state is characterized by nearly force-free fields, $\nabla\times B=\lambda B$, in which the radial profile of the parallel current tends to be nearly uniform in space; i.e., $\lambda = \mu_0 J_{||}/B$ is a constant. This allows for a stable equilibrium, in which there is no available free energy for current-driven tearing modes, with arbitrarily large magnetic field and current density for a given source current (that is, $J_{||}$ and B increase together). In principle, the spheromak current and field can grow until resistive dissipation balances the source input.

The Sustained Spheromak Physics Experiment (SSPX) [3] was designed to address both magnetic field generation and confinement. Confinement improvements in SSPX give peak T_e~350 eV and core electron thermal diffusivities of $\chi_e<10$ m^2/s, and most SSPX temperature data is bounded by a β_e~5%. Given a limiting beta, an increase in temperature is obtained by increasing the magnetic field strength ($T\sim\beta B^2$), which motivates our experimental efforts reported here. If it can be shown that confinement scales favorably with magnetic field

strength [4] and spheromaks can be produced efficiently, then the spheromak would be an attractive magnetic fusion concept [5].

In this paper we discuss our recent experimental results that have led to an increased understanding of energy confinement and magnetic field generation in the spheromak. In Section 2 we present an overview of the SSPX device and operation. In Section 3 we discuss the elements necessary to achieve improved operation in SSPX, and in Section 4 we discuss energy confinement. Section 5 covers magnetic field generation and a review of theoretical understanding is presented in Section 6. Finally in Section 7 we present a summary and discuss future work.

2. Overview of the SSPX device and operation

The SSPX device produces 1.5 – 4.0 ms, 1 m diameter by 0.5 m high spheromak plasmas with a plasma minor radius of 0.23 m and major radius of 0.31 m. Fig. 1 shows a cross section of the SSPX identifying the major hardware components along with a typical MHD equilibrium. As in CTX [6] and earlier spheromak experiments [1], DC coaxial helicity injection is used to build and sustain the spheromak plasma within the flux conserver. In SSPX, the outer electrode of the coaxial region is contiguous and electrically connected to the outer flux conserver. The plasma-facing surfaces of the copper flux conserver are tungsten-coated (100μm thick) to reduce sputtering.

The vacuum "bias" flux configuration for the coaxial injector is quite flexible in SSPX, as shown with two examples in Fig. 2. In the standard configuration (Std), the magnetic field is largely confined to the coaxial region ($B_r \sim 200$ gauss), whereas in the Modified Flux (MF) configuration, vacuum field lines extend into the flux conserver. In both cases, there is a small "Penning region" near the inner electrode that helps obtain breakdown at lower gas pressure. In either configuration, a spheromak plasma is formed when we inject gas into the coaxial region and apply –7-10 kV to the inner electrode (the discharge cathode). The resulting

plasma is rapidly ejected into the flux conserver when the current rises above the ejection threshold after ~150 μs. The ejection threshold current depends on the strength and configuration of the vacuum magnetic field; the MF flux configuration has a lower, less-well defined threshold current than the Std case because the field strength in the coaxial region decreases smoothly towards the mouth of the injector.

The toroidal current and internal magnetic field profiles of the resulting spheromak plasma are inferred from edge poloidal magnetic measurements using the CORSICA code [3] to reconstruct the 2d MHD equilibrium, assuming that $\lambda=\mu_0 J/B$ is a flux function of the form $\lambda= \lambda_{edge}(1+\alpha\psi^n)/(1+\alpha)$, where $\lambda_{edge}= \lambda_{gun}=I_{gun}/\psi_{gun}$. CORSICA includes plasma current on the open field lines when generating the equilibrium; a typical reconstruction appears in Fig. 1. The mean λ of the spheromak matches the Taylor state geometric eigenvalue of the flux conserver [7], $\lambda_{FC}=9.9 m^{-1}$, as expected. The edge field (B_{pol} and B_{tor}) is measured around the boundary at 20 locations that span the complete poloidal cross section from above the injector X-point to the bottom of the flux conserver and include a toroidal array at the midplane. The typical RMS error between the probe data and predictions from the computed MHD equilibrium are in the range of 4-6%. The magnetic probes also provide information on magnetic fluctuations.

The spheromak plasma ejected by the formation pulse decays resistively with a time constant of several milliseconds. However, since the electron temperature (T_e) is lower at the edge than at the magnetic axis, the spheromak current profile gradually becomes more peaked leading to instability, loss of global MHD equilibrium, and abrupt collapse after only 1.5 ms or so. The onset of this instability can be avoided by maintaining the edge current.

In SSPX we use a second capacitor bank (a sustainment bank) to apply a 3 ms flat-top current pulse to maintain the spheromak plasma after it has been formed in the flux conserver; this bank is configured as a five-section pulse-forming L-C network (PFN). The peak current

and shape of this *sustainment* pulse is set by the circuit parameters of the PFN, not the impedance of the spheromak plasma: the bank acts as a constant current power supply for the spheromak. Use of the word *sustainment* can imply steady state conditions; however, during the sustainment phase of the discharge in SSPX, the magnetic field is actually decaying slightly. In Fig. 3 we show representative discharges with (red) and without (black) the sustainment pulse. The dashed line in the top window shows the current from the sustainment bank, while the bottom window shows how the spheromak lifetime is extended by addition of the sustainment pulse. The middle box shows the voltage on the inner electrode, which is determined by the plasma impedance.

3. Steps to improved performance

A key element to achieving high performance discharges on SSPX is current profile control to minimize magnetic fluctuations. We vary the timing and amplitude of the sustainment pulse to provide rough control of the current profile in the spheromak, using $\lambda_{gun}=I_{gun}/\psi_{gun}$ as the figure of merit. Here we use the total bias magnetic flux (ranging up to 50 mWb) to define ψ_{gun}. Inside the magnetic separatrix, λ is nearly constant, $\lambda \sim \lambda_{FC}$. Thus, when we operate with $\lambda_{gun} > \lambda_{FC}$, we expect to find "hollow" current profiles, borne out by CORSICA MHD equilibrium reconstruction. Similarly, when operating with $\lambda_{gun} < \lambda_{FC}$, we expect "peaked" current profiles, also as found by CORSICA. When $\lambda_{gun} \cong \lambda_{FC}$, the current profiles should be fairly flat. Typically, we apply the sustainment pulse so that the current reaches steady state about the time that the spheromak magnetic field reaches its peak value (~300 μs) and before the edge instability begins to grow, as shown in Fig. 3.

By optimizing the edge current relative to the injector flux, fluctuation levels are reduced to less than 1%. Fluctuation levels are lowest when the injected edge current is maintained at a level sufficient to keep the radial current density profile flat to slightly peaked. When the edge current is increased, then fluctuation levels increase with a corresponding decrease in

confinement. If the edge current is not maintained, then the current profile relaxes, becoming unstable to an n=2 mode, and the magnetic equilibrium collapses. Figure 4 is a plot of the core electron temperature as a function of the normalized current density, or λ_{gun}. In this scan, the capacitor bank was operated with constant conditions (constant I_{gun}) and the bias flux was varied (maintaining a "modified flux" configuration), thereby maintaining constant input power and helicity. The flux variation thus is represented as a variation in $\lambda_{gun}=\mu_0 I_{gun}/\psi_{gun}$. When $\lambda_{gun}=\lambda_{fc}$ the current density profile is kept close to the relaxed state, λ= constant. As the free energy for current-driven modes is proportional to the gradient of λ, the magnetic modes then relax to low amplitudes allowing magnetic surfaces to form. Experimentally, the highest electron temperatures are obtained when the current profile is slightly peaked; Ohmic heating in the core plasma is higher than in the flat limit and fluctuation levels remain low as the q-profile does not span low-level rational surfaces.

It is also important to control impurity radiation and recycling in order to minimize helicity dissipation. Therefore, wall conditioning is another key element in obtaining reproducible high temperature discharges in SSPX. After a major vent, the machine is baked to 165^{o}C to remove water and hydrogen, followed by glow discharge cleaning (GDC) to remove surface hydrocarbons and oxides. Baking at 165^{o}C for ~100 hours reduces the partial pressure of water by an order of magnitude. Hydrogen GDC after the bake produces only a modest further reduction in water content due to the limited pumping speed (500 liters/sec) and high backfill pressures (30 mTorr) needed to clean the injector region.

Even with baking and GDC the partial pressure of water can increase significantly after the start of plasma operations, sometimes equaling the partial pressure of the hydrogen fuel gas. Other gases (methane, carbon monoxide and carbon dioxide) are also produced during these discharges. Water and volatile gas production during plasma discharges is attributed to the reduction of tungsten compounds (i. e., tungsten oxide) by hydrogen. To reduce the

production of water and volatile gases, helium shot conditioning is employed. The SSPX vessel is backfilled with ~4 mTorr of helium, and ~10-12 helium fueled discharges are required to decrease the partial pressure of water and volatile gases an order of magnitude.

Another key element to producing high temperature discharges is density control. Discharges on SSPX are sensitive to the plasma density and impurity content since low temperature resistive plasmas have lower confining magnetic fields and corresponding worse confinement than hotter plasmas because currents in the plasma produce the fields. A key measure for the spheromak is the quantity I/N (equivalently j/n), which can be related to the ratio of Ohmic heating input power to impurity radiation loss power. As long as j/n is greater than ~10^{-14} A-m, the Ohmic heating will exceed the impurity radiation loss.

During the sustained operations the density depends strongly on whether the sustaining current is above the spheromak formation threshold, $\lambda=I/\psi$. If below threshold, then there is only a weak dependence on λ since most of the current and plasma remain in the injector region. As the current rises above the threshold, the injector plasma is swept out into the main chamber and the spheromak density attains high levels. Global particle balance studies show that less than 1% of the hydrogen fueling gas is retained in the tungsten walls after a plasma pulse. However, due to the porous nature of the tungsten surface, it takes many minutes for the hydrogen to be pumped away after it diffuses back to the surface and this leads to higher recycling; higher recycling leads to higher density. Therefore, density control is obtained with the use of titanium gettering to trap the hydrogen more effectively and reduce the recycling. With gettering, we maintain low concentrations of low-Z impurities and steady line averaged density of ~5x1019 with a toroidal current of ~ 600kA.

The time history of a representative SSPX discharge with good confinement is shown in Fig. 5. This representative discharge was obtained by paying careful attention to wall conditioning (gettering every 3-4 shots) and density control; without gettering the density and

impurity radiation begin to rise at the end of a discharge. Discharges with the highest measured T_e ~350 eV and lowest core thermal diffusivity (χ_e < 10 m^2/s) occur when the injected current and gun flux are optimized to maintain a slightly peaked current profile. Careful optimization of the injected current also reduces the edge magnetic fluctuation amplitude ($|\delta B/B|_{rms}$~0.5%). Spatial profiles of T_e and χ_e during the time of the discharge when the edge fluctuations are at a minimum for several high performance discharges are shown in Figures 6 and 7 respectively.

4. Energy confinement

Global energy confinement ($\tau_E=\int nkTdV/P_{in}$) in spheromaks has always been short compared to comparable-sized tokamaks. This largely results from the fact that, in the spheromak, most of the plasma input power is dissipated in producing the confining magnetic field by edge currents in the plasma itself, whereas the magnet power is neglected in calculating τ_E for the tokamak (hence the term "scientific breakeven"). In a spheromak reactor, the edge Ohmic power dissipation should be small compared to the core fusion power [8]. Thus, we have focused on using the core thermal diffusivity as a fundamental figure of merit for evaluating the confinement properties of the spheromak. (The core thermal diffusivity is determined by solving $n_e\chi_e\nabla T_e\big|_s=\int_s P_{ohmic}dV$, where s defines the flux surface on which the gradient is evaluated and inside of which the total Ohmic power is computed). In this way we can make direct comparison to other toroidal confinement devices without having to account for all the operational and geometrical properties of the configuration.

We determine the electron thermal diffusivity in the SSPX from the electron power balance computed at the time when T_e peaks and dE/dt =0. Impurity spectroscopy shows Ti ~ Te during this phase of the discharge, so we neglect the ions in this analysis and consider resistive dissipation as the sole source of electron heating in the confined plasma. Impurity

radiation typically amounts to less than 20% of the total input energy and since we do not have internal emissivity profiles, we also neglect impurity radiation in the power balance.

We compute the Ohmic heating power on internal flux surfaces from ηj^2, using the CORSICA code to determine j(r) from the MHD equilibrium, as inferred from magnetic probe measurements of the poloidal magnetic field at the flux conserver. The equilibrium reconstruction is further constrained by matching the computed current on open field lines to the measured gun current. We use the classical Spitzer electrical resistivity, computed from the electron temperature and density measured by Thomson scattering, along with a spatially uniform Z_{eff}~2.5 estimated from VUV spectroscopy and the magnetic field decay times. The underlying physics controlling confinement and transport in spheromaks is subject to ongoing study, especially in the "best" regimes with highest temperature and lowest transport. In these regimes, we observe a large difference between transport in the core and near the separatrix (Fig. 7) indicating different mechanisms may be dominating in each region. In the core, energy transport approaches tokamak levels with electron temperatures over 350 eV and peak electron beta of 5%, but the edge Te is ~50 eV. Thermal diffusivity (χ_e) at the magnetic axis is less than 10 m^2/sec, but increases to over 100 m^2/sec at the separatrix. The scaling studies of χ_e vs. Te, shown in Fig. 8, are an initial step in the process to identify which of several transport models might apply and under what conditions. In hot plasmas, the perpendicular electron thermal conductivity, χ_e, drops by two orders of magnitude between 50 eV and 350 eV.

5. Magnetic field generation

Progress has been made in understanding the mechanisms that generate fields by helicity injection. Simple helicity balance suggests that the spheromak magnetic fields are limited only by dissipation. The complete ensemble of SSPX discharges show that the edge poloidal magnetic field (and thus the toroidal current) scale linearly with the injected current. These

data appear in Fig. 9, where we plot the peak midplane edge poloidal field vs. the peak injector current.

Also shown in Fig. 9 are two operating modes (previously reported [9,10]) observed to increase the magnetic field: (A) "Slowly-building" operation with constant current and spontaneous gun voltage fluctuations. In this case, the gun is operated continuously at the threshold for ejection of plasma from the gun: stored magnetic energy of the spheromak increases gradually with $\delta B/B$ ~2% and large voltage fluctuations (δV~1 kV), giving a 50% increase in current amplification, I_{tor}/I_{gun} [9]. (B) "Double-pulsed" operation with controlled current pulses. In this case, spheromak magnetic energy increases in a stepwise fashion by pulsing the gun, giving the highest magnetic fields observed for SSPX (~0.7 T along the geometric axis) [10]. In each case, the processes that transport the helicity into the spheromak are inductive and exhibit a scaling of field with current that exceeds those previously obtained (blue dots in Fig. 9). Fig. 9 provides an equivalent figure of merit to current amplification, the peak edge poloidal field per MA of gun current. Typical SSPX operation obtains B_{pol}=0.65T/MA (blue line), whereas the "slowly-building" operating modes reach nearly 1T/MA (red line). Newly found scalings suggest how to achieve higher temperatures with a series of pulses [11].

Experimentally we have found it is possible to steadily build the helicity content of the spheromak by applying a relatively "square" pulse of gun current such that the injector λ is larger than the flux conserver eigenvalue. Originally, we chose a configuration with a "soft" formation threshold current to minimize the likelihood of driving a large n=1 central column mode. The mode amplitude is minimized by keeping the initial current as low as possible, consistent with increasing the poloidal flux, making this a robust operating mode. Under these conditions, there is a positive gradient in normalized current density $\lambda=\mu_0 j/B$ going from the magnetic axis to the edge of the spheromak. Such discharges are characterized by continuous

large high frequency, incoherent voltage fluctuations with a concomitant rise in DC gun voltage. The net result is an increased time-average helicity input and steadily rising spheromak magnetic field that reaches a peak of 1Tesla/MA when the bank runs out of charge. Figure 10 is a plot of the range of bias magnetic field configurations for which we observe this kind of operation.

The nature of the reconnection processes responsible for the continuous helicity injection is still an open question. The strongest cross-correlation between the voltage and field fluctuations is for the field in the coaxial gun region, from which it was inferred that the gun was ejecting current filaments that would then merge into the spheromak [9]. 3D resistive MHD simulations with the NIMROD code (discussed in Section 5 below) of discharges with similar current waveforms also exhibit large voltage spikes, which are correlated with current sheets and reconnection near the injector x-point region. It may also be that the filamentation and reconnection actually occurs around the boundary of the central column.

6. Summary of present theoretical understanding

Numerical simulation closely coupled to the experiment, has significantly improved our understanding of spheromak operation. While details of many of these results have appeared elsewhere, we present salient results here for completeness. 3D resistive MHD simulations with the NIMROD code for conditions similar to SSPX single and double pulse discharges with increasingly realistic representations of the gun geometry, magnetic bias coils, and current drive pulse histories, and with Braginski temperature-dependent thermal conductivities are tracking the reconstructions of the magnetic configuration, and the temperature and magnetic fluctuation histories with increasing fidelity [12-15]. We are continuing NIMROD simulations addressing different current-drive pulsing strategies, the influence of a conducting insert, and the physics of magnetic reconnection in spheromak formation [15,16]. The effects of magnetic field fluctuations on the quality of confinement in

SSPX have been studied in Monte Carlo calculations [17] using model magnetic field perturbations added to the spheromak equilibrium field as derived from edge magnetic probe data using CORSICA. Similar physics has been addressed directly in the NIMROD self-consistent simulations [12-17]. The non-axisymmetric magnetic fluctuations in SSPX are determined by probes at the edge of the plasma to be a few percent [18]. Poincaré puncture plots show that a perturbation strength $\delta B/B > 3-5\%$ in the non-self-consistent Monte Carlo computations leads to a dramatic degradation of confinement due to formation of magnetic islands and stochastic field regions, and this is supported by NIMROD simulations [14-15].

7. Summary and future work

In a magnetized coaxial gun-driven spheromak current drive is provided by a plasma dynamo: external currents flowing at the edge on open field lines couple to internal currents flowing on closed or nearly closed flux surfaces. Magnetic fluctuations are observed at both high and low edge currents. These fluctuations are responsible for both energy input associated with Ohmic heating and energy loss through heat transport out of the core to the edge. When the external current drive is high, a kinked distortion (n=1 mode) is observed on the open field lines. This n=1 mode provides the fluctuation power that couples current from the open magnetic flux to the spheromak. When the edge currents are reduced higher order modes are observed and result in resistivity-profile effects that lead to a collapse of the magnetic equilibrium. By optimizing the edge current relative to the injector flux, fluctuation levels are reduced to less than 1% leading to a nearly quiescent regime giving peak T_e~350 eV and core electron thermal diffusivities of χ_e<10 m^2/s.

The primary goal of the SSPX is to test whether favorable energy confinement scaling can be obtained in a spheromak plasma sustained by coaxial helicity injection. This requires that we produce adequate magnetic field to obtain high-temperature plasmas. Experiments now underway will more fully examine the correlation between high temperatures and low

magnetic fluctuations and we are working on designing a new, small diameter coaxial injector to test several theories of magnetic field generation. A previous modification to the power system extended the pulse length a factor of four (from ~1 ms to 4 ms) and the peak magnetic field strength more than doubled, to 0.4 T. Presently, we are constructing a modular capacitor bank to (1) add increased flexibility in programming the shape of the current pulse, (2) extend the pulse length to ~12 ms and (3) double the available gun current which will double the energy coupled to the spheromak by minimizing coupling losses due to impedance mismatch.

A series of shots were analyzed to determine the scaling of T_e with B. These shots had low impurities and similar T_e profiles. Parameters scanned were formation gun flux and current producing shots with $B_{edge} = 0.1$ to 0.35 T. Results (Fig. 11) show a very clear correlation of $T_e \sim B^2$. These data show evidence for a limiting β, but we cannot differentiate between a stability limit and simple energy transport limit (as discussed below). It should be noted that our highest temperature discharges are obtained using the maximum current available from the existing capacitor banks. The new modular bank will allow us to double the injected current and should lead to a further increase in T_e.

The latest results provide strong motivation for adding auxiliary heating to the SSPX device in order to significantly advance our understanding of how the spheromak works. Until now, spheromak plasmas were heated solely by resistive dissipation (so-called Ohmic heating); i.e., the same internal current that produces the confining magnetic field also provides the heat input via the temperature-dependent plasma resistivity ($\eta \propto T^{-3/2}$). The Ohmic heating power in the core plasma ($r/a < 0.5$) can be 10 MW or more in cold spheromak plasmas, but it decreases rapidly with temperature, dropping to less than 1.5MW in 300eV SSPX discharges. Thus, in the SSPX spheromak for the first time it becomes possible to consider adding modest (1-2MW) auxiliary heating power to change the local power balance and plasma temperature.

The addition of NBI heating to change the core plasma power balance represents a significant step forward in spheromak research for several reasons. The fact that the heat input depends on the impurity content (Z_{eff}) and decreases strongly with the electron temperature complicates the transport analysis, in which we solve the steady-state energy balance for the electron thermal diffusivity χ_e. Furthermore, these dependencies make discovering the independent variables that govern energy transport in the spheromak (such as magnetic field B) problematic. Adding an external heat source which is independent of the plasma current and whose spatial location is well known, dramatically improves analysis capability, reduces uncertainties, and removes dependent variables.

Auxiliary heating will also allow us to explore the experimental pressure limit of the spheromak configuration for the first time by providing independent control of the plasma pressure and magnetic field. The ratio of the plasma pressure to the magnetic field pressure ($\beta=2\mu_o nkT/B^2$) is an important measure of the efficiency of a magnetic fusion power plant, and every magnetic field configuration has a maximum β for which the plasma maintains MHD stability. SSPX data show evidence for a limiting β, but we now cannot differentiate between a stability limit and simple energy transport due to relationships between current, input power, and magnetic field as outlined above. The ability to add heat at fixed field provided by auxiliary heating will provide a clean experimental test for the first time.

Acknowledgements

This is a report of work supported by the US Department of Energy under Contract No. W-7405-ENG-48. The authors wish to acknowledge and thank B. Cohen, R. Cohen, G. Cone, K. Fowler, T. Kopriva, L. LoDestro, L. D. Pearlstein, D. Ryutov, C. Sovinec, and M. Umansky for numerous technical contributions and encouragement.

This work was performed under the auspices of the U.S. Department of Energy by University of California, Lawrence Livermore National Laboratory under contract W-7405-Eng-48.

References

[1] T. R. Jarboe, Plasma Phys. and Control. Fusion **36** 945 (1994).

[2] B. Taylor, Rev. Mod. Physics **58** 741 (1986).

[3] E. B. Hooper, L.D. Pearlstein, and R.H. Bulmer, Nucl. Fusion **39** 863 (1999).

[4] T. K. Fowler Fusion Tech. **29** 206 (1996).

[5] E. B. Hooper, *et al.*, Fusion Tech. **29** 191 (1996).

[6] C.W. Barnes, *et al.,* Phys. Fluids B **2** 1871 (1990).

[7] W.C. Turner, *et al.*, Phys. Fluids **26** 1965 (1983).

[8] R. L. Hagenson, R. A. Krakowski, Fusion Technol. **8** 1606 (1985).

[9] S. Woodruff, *et al.*, Phys. Rev. Lett. **90** 095001 (2003).

[10] S. Woodruff, *et al.*, Phys. Rev. Lett. **93** 205002 (2004).

[11] S. Woodruff, *et al.*, Phys. Plasmas **12** 052502 (2005).

[12] R.H. Cohen, *et al*., Nucl. Fusion **43** 1220 (2003).

[13] C.R. Sovinec, J.M. Finn, and D. Del-Castillo-Negrete, Phys. Plasmas **8** 475 (2001).

[14] C. R. Sovinec, *et al*., Phys. Plasmas **10** 1727 (2003).

[15] C.R. Sovinec, *et al*., Phys. Rev. Lett. **94** 035003 (2005).

[16] B.I. Cohen, *et al*., Phys. Plasmas **12** 056106 (2005).

[17] E. B. Hooper, *et al*., "Magnetic reconnection during flux conversion in a driven spheromak", accepted for publication, Phys. Plasmas (August, 2005).

[18] H. S. McLean, *et al*., Phys. Rev. Lett. **88** 125004 (2002).

Figure captions

Fig. 1. Cross section of the SSPX spheromak showing main hardware components with MHD equilibrium superimposed. Outer electrode/flux conserver is 1m in dia. and diameter of the inner electrode is 0.68m.

Fig. 2. Bias vacuum magnetic flux for standard (Std) and Modified (MF) flux configurations. Contour lines every 2mWb for 34mWb total bias flux.

Fig. 3. Representative SSPX discharges. 3370 (black)-formation pulse only, 6937 (red)-with sustainment bank.

Fig. 4. Core electron temperature as a function of the normalized current density, or λ_{gun}. T_e is highest and fluctuation amplitudes are lowest when the current density profile is slightly peaked (to the right of the shaded region where $\lambda_{gun}=\lambda_{fc}$). Increasing λ is to the left.

Fig. 5. Time evolution of high T_e shot; (a) injected gun current, (b) electron density, (c) edge poloidal field at the midplane, (d) edge magnetic fluctuations $|\delta B/B|_{rms}$. Fluctuations are lowest during the shaded time band.

Fig. 6. Spatial profiles of T_e as a function of radius for 6 high performance discharges

Fig. 7. Thermal diffusivity, χ_e, as a function of normalized radius r/a, a=17cm, for 5 high performance discharges.

Fig. 8. Electron thermal diffusivity, χ_e, for an ensemble of SSPX discharges.

Fig. 9. Edge field scaling with I_{gun} for fast formation plasmas (blue), for the slow build-up cases (red circles), and double pulse operation (large green circle).

Fig. 10. Slow-start steady buildup has been extended to several bias magnetic field configurations.

Fig. 11. Scaling of Te with B.

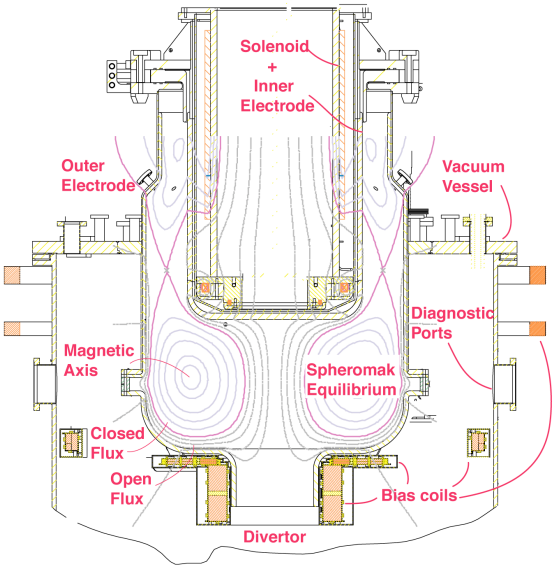
Solenoid
+
Inner
Electrode
Outer
Electrode
Vacuum
Vessel
Diagnostic
Ports
Magnetic
Axis
Spheromak
Equilibrium
Closed
Flux
Open
Flux
Bias coils
Divertor

Wood, Fig. 1

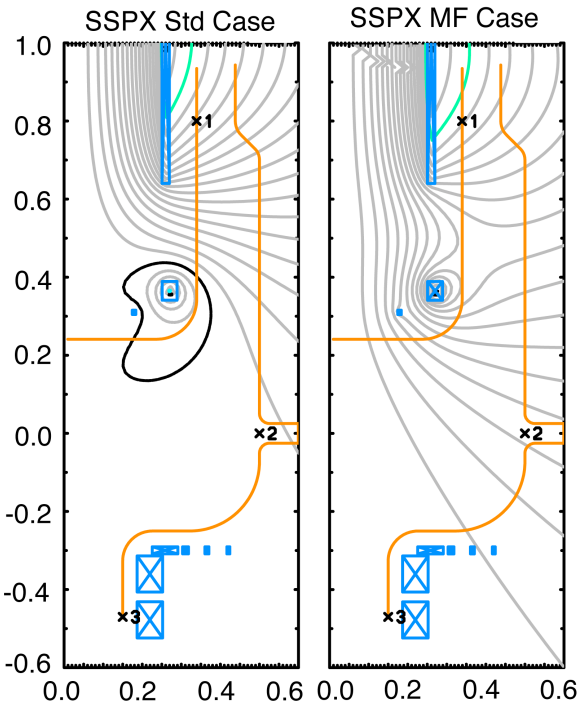
SSPX Std Case
SSPX MF Case
1.0
0.8
0.6
0.4
0.2
0.0
-0.2
-0.4
-0.6
0.0
0.2
0.4
0.6
×1
×2
×3

Wood, Fig. 2

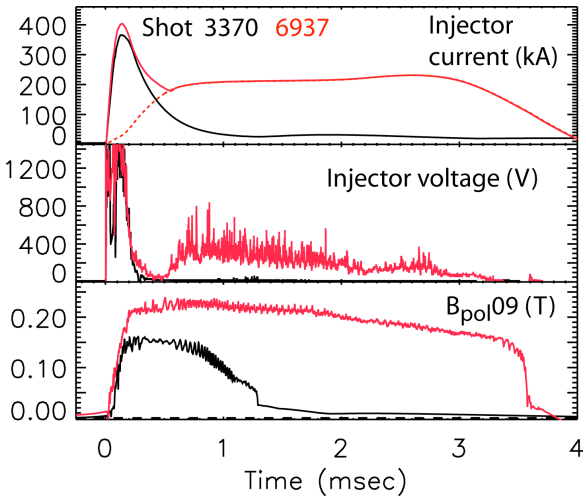
Shot 3370 6937
Injector current (kA)
400
300
200
100
0
Injector voltage (V)
1200
800
400
0
$B_{pol}09$ (T)
0.20
0.10
0.00
0
1
2
3
4
Time (msec)

Wood, Fig. 3

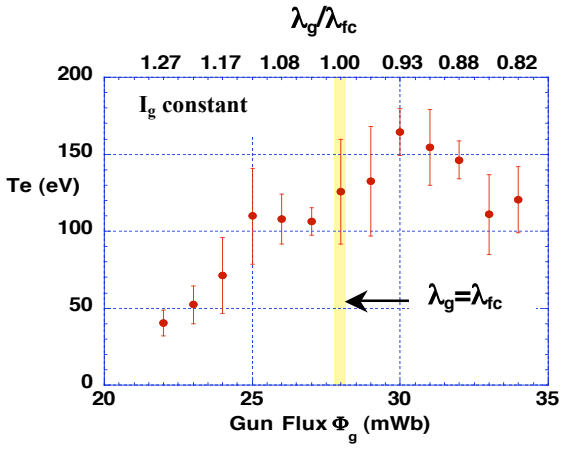
λg/λfc
1.27 1.17 1.08 1.00 0.93 0.88 0.82
200
150
100
50
0
Te (eV)
Ig constant
λg=λfc
20 25 30 35
Gun Flux Φg (mWb)

Wood, Fig. 4

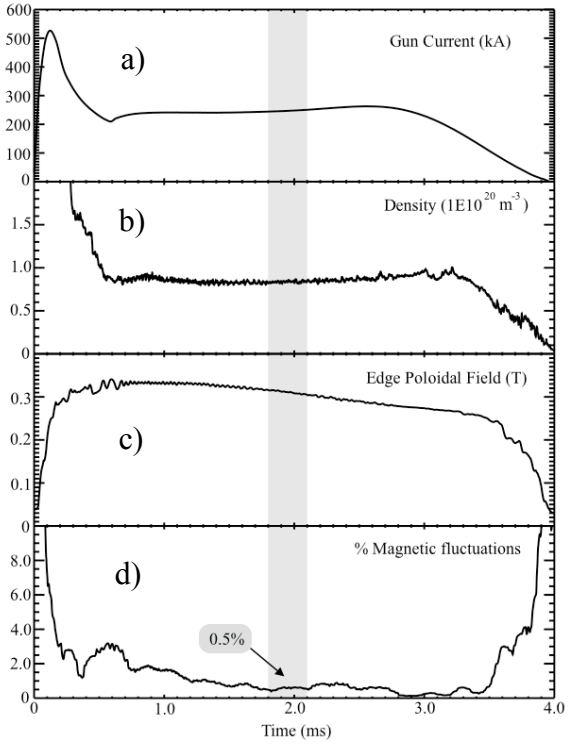
a)
Gun Current (kA)
b)
Density (1E10 20 m -3)
c)
Edge Poloidal Field (T)
d)
% Magnetic fluctuations
0.5%
Time (ms)

Wood, Fig. 5

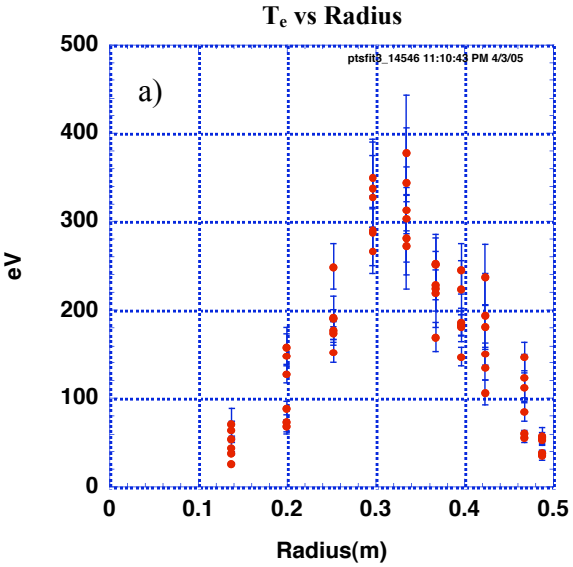
T_e vs Radius
ptsfit3_14546 11:10:43 PM 4/3/05
a)
500
400
300
200
100
0
eV
0
0.1
0.2
0.3
0.4
0.5
Radius(m)

Wood, Fig. 6

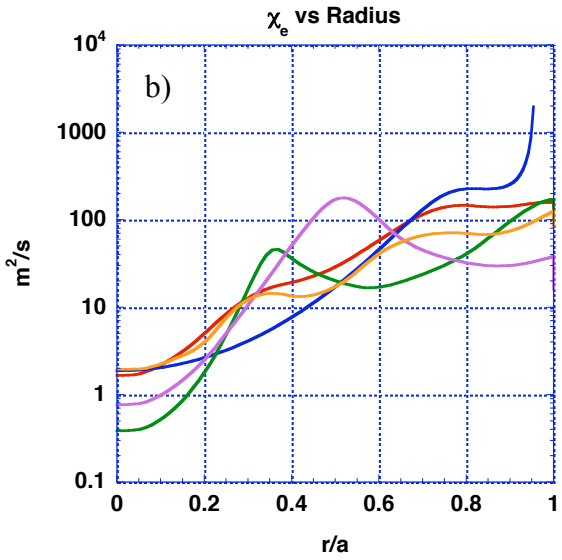

Wood, Fig. 7

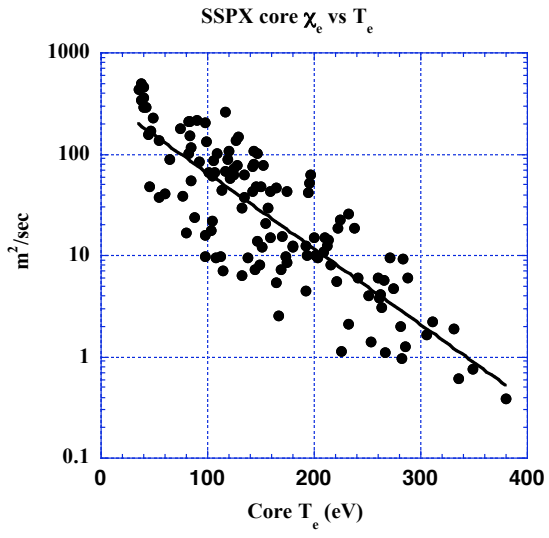
SSPX core χ_e vs T_e
1000
100
10
1
0.1
m^2/sec
0
100
200
300
400
Core T_e (eV)

Wood, Fig. 8

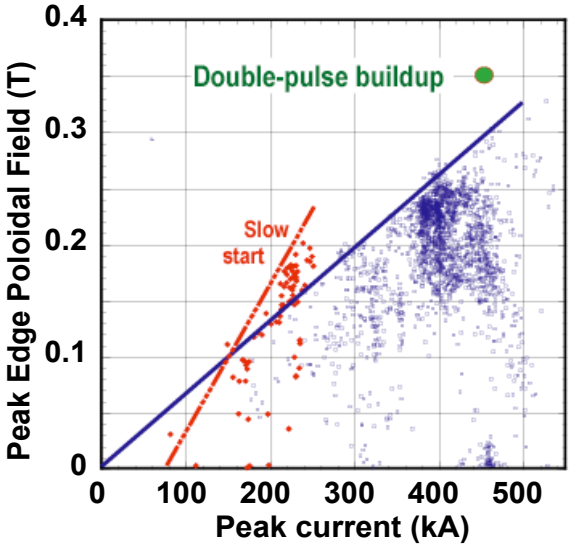
Peak Edge Poloidal Field (T)
0.4
0.3
0.2
0.1
0
Double-pulse buildup
Slow
start
0
100
200
300
400
500
Peak current (kA)

Wood, Fig. 9

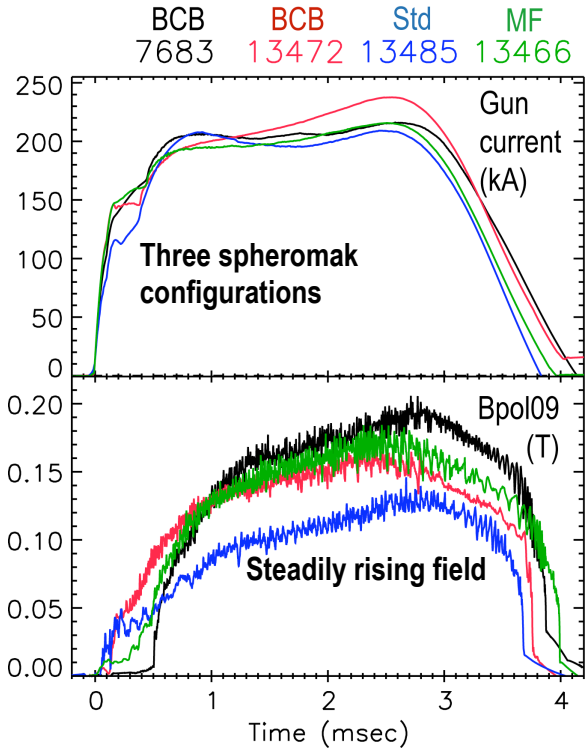
BCB
7683
BCB
13472
Std
13485
MF
13466
250
200
150
100
50
0
Gun
current
(kA)
Three spheromak
configurations
0.20
0.15
0.10
0.05
0.00
Bpol09
(T)
Steadily rising field
0
1
2
3
4
Time (msec)

Wood, Fig. 10

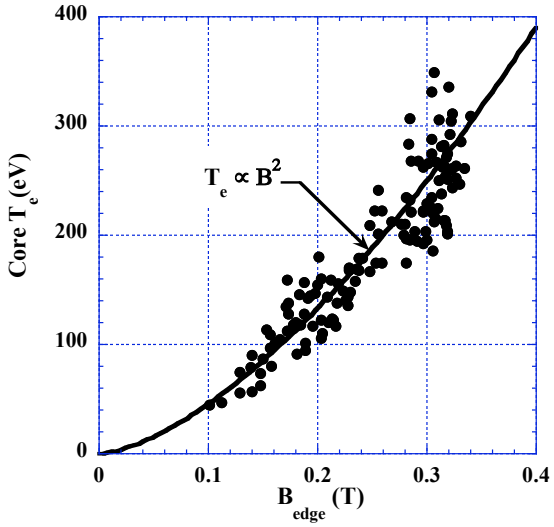

Wood, Fig. 11